JOURNAL OF MATERIALS SCIENCE 19 (1984) 1726–1736

Diffraction studies of ß″-magnesium sialon

G. LENG-WARD
Department of Science, Polytechnic of Wales, Pontypridd, UK

M. H. LEWIS
Department of Physics, University of Warwick, Coventry, UK

S. WILD
Department of Civil Engineering and Building, Polytechnic of Wales, Pontypridd, UK

The compositions of high magnesium content β''-magnesium sialon crystals within the $3M/4X$ plane of the Mg–Si–Al–O–N system indicate some form of metal atom ordering wihtin the β'' structure. Although it is not possible using X-ray diffraction to detect weak additional reflections arising from the ordering between magnesium, aluminium, and silicon atoms, such weak reflections are revealed on electron diffraction photographs for a β'' phase, resulting in a tripling of the hexagonal lattice c-dimension. These show β'' to have a structure very similar to rhombohedral willemite (Zn_2SiO_4), with the (Mg, Al) metal atoms ordered with respect to the silicon atoms in a 2:1 ratio. However, there are some additional weak diffraction spots with indices not obeying the rhombohedral condition of $-h + k + l = 3n$. It is proposed that the structure of this β'' is identical to that of willemite and the extra spots are a result of some form of twinning, which implies the existence of "ordered microdomains".

1. Introduction

The structure of β-Si_3N_4 [1, 2] is described by the hexagonal space group $P6_3/m$. Aluminium and oxygen are able to substitute into β-Si_3N_4 forming a solid solution termed β'-sialon [3, 4], according to the formula $Si_{6-z}Al_zN_{8-z}O_z$ with the solubility limit given by Jack [3] as $z \sim 4.2$ (see Fig. 1). Now the arrangement of metal and non-metal atoms in β-Si_3N_4/β' sialons is identical with that in phenacite-type compounds such as Be_2SiO_4 [5] and Zn_2SiO_4 [6]. Both these phenacite-type compounds belong to the rhombohedral space group $R\bar{3}$ because of the decrease in symmetry resulting from the metal atom ordering in the ratio of 2:1 of the beryllium and silicon atoms in beryllium silicate, and the zinc and silicon atoms in the zinc silicate.

The composition of the $z = 4$ sialon is $Al_2SiO_2N_2$, which is the same as the phenacite composition (neglecting the fact that there are two types of non-metal atoms) and one might expect phenacite-type ordering between the aluminium and silicon atoms. However, X-ray and electron diffraction photographs of $z = 4$ sialon and neutron diffraction studies by Gillot *et al.* [7] show no evidence for any ordering between the aluminium and silicon atoms in $z = 4$ sialon. This is either because there is no such ordering, or because the difference in scattering factors between aluminium and silicon is too small to produce observable additional "superlattice" reflections; although Gard and co-workers [8, 9] have found that silicon and aluminium ordering, in tetrahedral sites, can be detected by electron diffraction in zeolite A and anorthite. The substitution of magnesium for aluminium in β'-sialons would make the detection of any metal atom ordering easier as the difference in scattering between magnesium and silicon is more significant, particularly for electrons at low angles.

Wild *et al.* [10] and Leng-Ward [11] have confirmed the existence of magnesium substituted β' sialons, termed β'', with a range of compositions in the $3M/4X$ plane of the Mg–Si–A–Al–O–N system (M-metal atoms, X-non metal atoms). β''-magnesium sialons may form by two distinct mechanisms:

0022–2461/84 $03.00 + .12

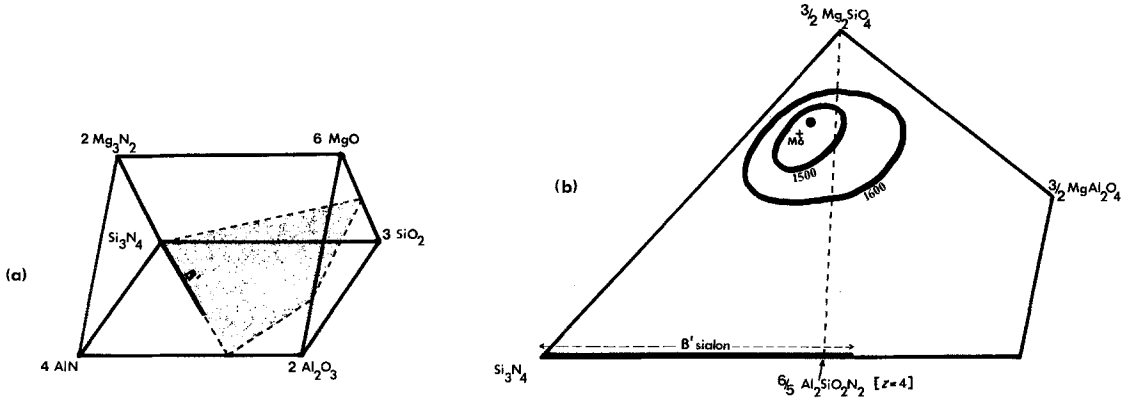

Figure 1 The MgSiAlON system (a), and (b) the $3M/4X$ composition plane of the MgSiAlON system showing the 1500 and 1600° C liquid isotherms, the eutectic (•) and M6 compositions. (M-metal atoms, X-non metal atoms).

(i) Low temperatue annealing of MgSiAlON ($3M/4X$) glasses. These glasses, obtained by quenching from the liquid state, must contain precipitated β-Si_3N_4/β' sialon nuclei for β'' nucleation and growth to proceed.

(ii) Coupled growth of low magnesium content β'' together with forsterite from slowly cooled MgSiAlON ($3M/4X$) liquids, producing a duplex microstructure.

The quenching of a MgSiAlON ($3M/4X$) liquid with a composition (M6) just on the Si_3N_4 side of the eutectic ($3M/4X$) liquid (see Fig. 1b) gives a glass containing a fine even distribution of β-Si_3N_4 crystals overgrown with a thin layer of β''. Annealing this glass in the temperature range 900 to 1000° C gives a metastable crystalline high magnesium content β'' glass–ceramic material stable up to approximately 1120° C [11]. EDAX (TEM) analyses of high magnesium content β'' crystals grown from a range of glass compositions [10] show a tendency for the β'' to crystallize at compositions approaching the Mg_2SiO_4–$Al_2SiO_2N_2$ join, i.e. the composition range given by the expression:

$$Mg_xAl_{4-x}Si_2O_{4+x}N_{4-x} \qquad (1)$$

This composition range is represented by the dotted line in Fig. 1b. The 2:1 ratio of (Mg, Al):Si throughout the composition range indicates a likely ordering of the magnesium and aluminium atoms with respect to this silicon atoms in the β'' structure, similar to that in phenacite-type compounds. X-ray and electron diffraction techniques are used in this work to try and detect additional reflections resulting from metal atom ordering in a β''-magnesium sialon.

2. Experimental techniques

2.1. Specimen preparation

All compositions in the $3M/4X$ plane of the MgSiAlON system are represented by the expression:

$$Mg_{m/2}Si_{6-z+(m/2)}Al_{z-m}O_zN_{8-z} \qquad (2)$$

An M6 pellet was prepared by grinding together appropriate proportions of dry MgO, SiO_2, Si_3N_4 and Al_2O_3 high purity powders (in an AGS mortar and pestle grinding machine) with an M6 composition of, $Mg_3Si_{2.455}Al_{0.545}O_{6.545}N_{1.455}$.

The powder was compacted into a 13 mm diameter cyclindrical pellet at a pressure of 2.25 MN m^{-2}. The weighed pellet was packed into boron nitride powder contained in a graphite crucible and reacted for 12 min at 1650° C in a static "oxygen free" nitrogen atmosphere. The liquid specimen was rapidly quenched by allowing the graphite crucible to drop out of the vertical furnace into a liquid nitrogen bath, giving a cooling rate of approximately 50° C sec^{-1} in the region 1650 to 800° C. Fragments of this quenched glass were crystallized as β'' by annealing in nitrogen between 900 and 1000° C.

2.2. Phase characterization, microstructure and diffraction

Crystalline phases were characterized by X-ray powder diffraction analysis employing a Guinier–Hagg focusing camera. Microstructure and phase morphology were determined by scanning and transmission electron microscropy (TEM).

TEM sections for imagining and diffraction were prepared by lapping thin specimen plates to 60 μm while attached to a glass slide, using

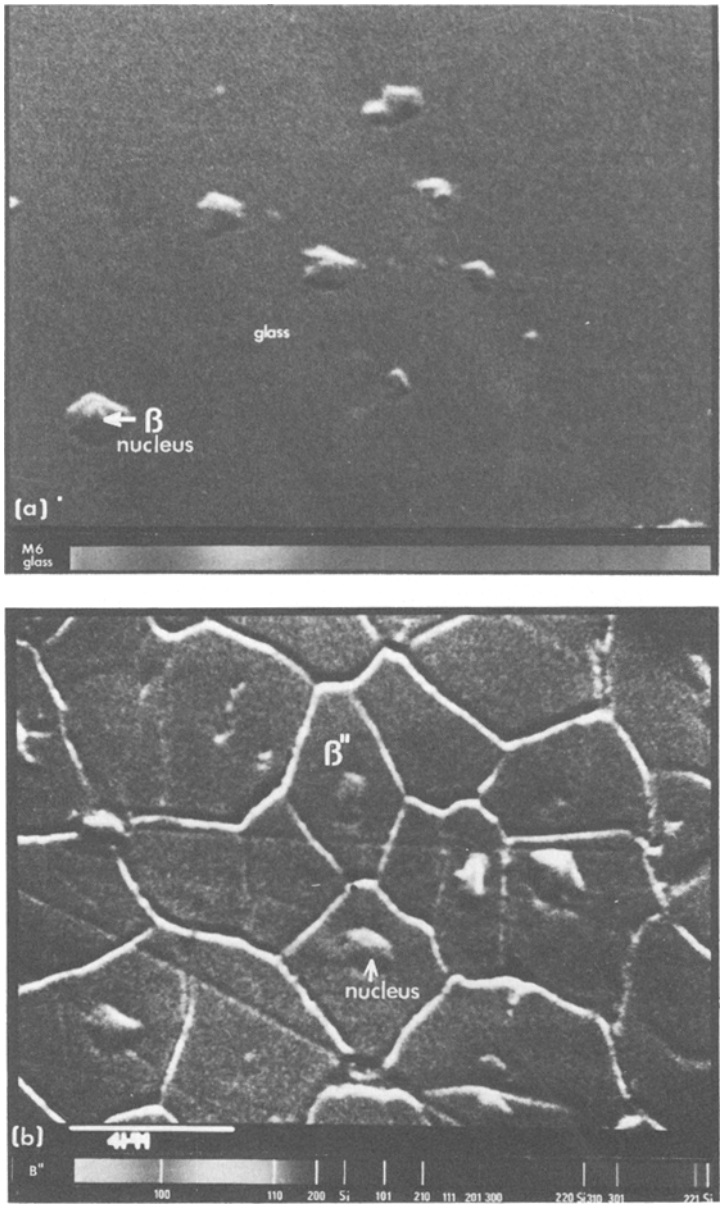

Figure 2 SEM micrographs and Guinier X-ray diffraction photographs of (a) quenched M6 glass, and (b) this glass annealed as β'' at 980° C.

silicon carbide abrasive paper on a polishing machine. These lapped sections were transferred to brass rings (3 mm diameter) and thinned to perforation using 5 kV argon ions incident at 40 degrees to both surfaces.

A willemite TEM specimen was prepared by grinding Zn_2SiO_4 powder suspended in a methyl acetate–colloidon solution in an agate mortar, giving a suspension of very thin Zn_2SiO_4 crystals many of which are electron transparent. A drop of this fine suspension was placed on a TEM copper grid which had previously had a continuous carbon film deposited on it.

3. Experimental observation and results

3.1. Microstructure

Fig. 2 shows SEM micrographs and Guinier X-ray diffraction photographs of (a) the quenched M6 glass containing β-Si_3N_4 nuclei; and (b) this glass after annealing as β'' as 980° C. The tendency for the β'' to crystallize at a composition slightly away from the glass composition towards the Mg_2SiO_4–$Al_2SiO_2N_2$ line together with the possibility that the glass is not exactly in the $3M/4X$ plane due to small weight losses (1.5 wt %) mean that the glass does not crystallize 100% as β'', but some residual glass is left at grain boundaries and triple points.

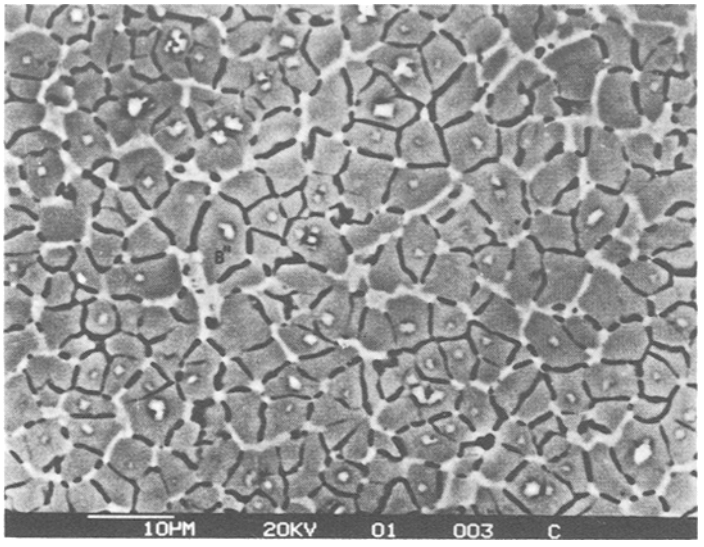

Figure 3 SEM (back scattered mode) micrograph of the M6 glass annealed as β''. Very light HF etch.

This residual glass shows up most clearly as the light phase in the lower magnification back-scattered mode SEM micrograph of Fig. 3. This residual glass together with the β-Si_3N_4 nuclei both show as light toned phases because they have compositions of higher average atomic number than the β''. The dark lines are β''/β'' boundaries that have been preferentially etched out into grooves by a very light HF etch, and return very little back-scattered signal.

3.2. X-ray diffraction

The M6 glass diffraction photograph in Fig. 2a shows only barely discernable lines from the crystalline nuclei present. The β'' X-ray diffraction photograph in Fig. 2b shows β'' reflections all of which index on the same hexagonal unit cell as β-Si_3N_4. There are no additional weak reflections resulting from metal atom ordering.

NB. There are three diffraction lines from a silicon standard added to the β'' sample, and, just to the left of the β'' 200 line is a very weak line attributable to the cellotape of the specimen holder.

3.3. Electron diffraction

3.3.1. Preliminary observations

Careful observation of long exposure electron diffraction photographs of the M6 β'', annealed at 910° C, reveals additional weak diffuse streaked spots along with the normal strong hexagonal β' pattern of spots. Two rows of these additional weak spots are only just visible (arrowed) in between the rows of strong spots in Fig. 4a. These diffuse spots, indicative of partial ordering, are too weak to be observable with the naked eye on the TEM screen.

However β'' crystals grown at 980° C shows a very marked sharpening of these additional spots, as shown in the two (110) electron diffraction patterns in Fig. 4, of β'' crystals grown at (a) 910° C and at (b) 980° C. These additional weak reflections reveal a form of long range ordering which results in a much larger hexagonal cell ($a_{\beta''}$, $c_{\beta''}$), nine times the volume of that originally used to index the X-ray powder diffraction patterns (a_β, c_β). The two cells are related by;

$$a_{\beta''} = 3^{1/2} a_\beta \qquad c_{\beta''} = 3c_\beta \qquad (3)$$

Phenacite-type compounds, being rhombohedral, can equally well be indexed on a similar large hexagonal cell [12]. When this is done, the hexagonal cell is no longer primitive but triple.

Willemite, Zn_2SiO_4, has very similar unit cell dimensions (large hexagonal cell) to the M6 β'' as is clearly shown in Table I. This similarity in cell dimensions means that the electron diffraction patterns of β'' and willemite are easily comparable. Therefore electron diffraction patterns of willemite were obtained in order to provide a direct comparison with those of β'' (for the same orien-

TABLE I Large hexagonal unit cell dimensions of β'' (M6) and willemite

Material	a (nm)	c (nm)
β''-magnesium sialon (M6)	1.364	0.9315
Zn_2SiO_4	1.394	0.9309

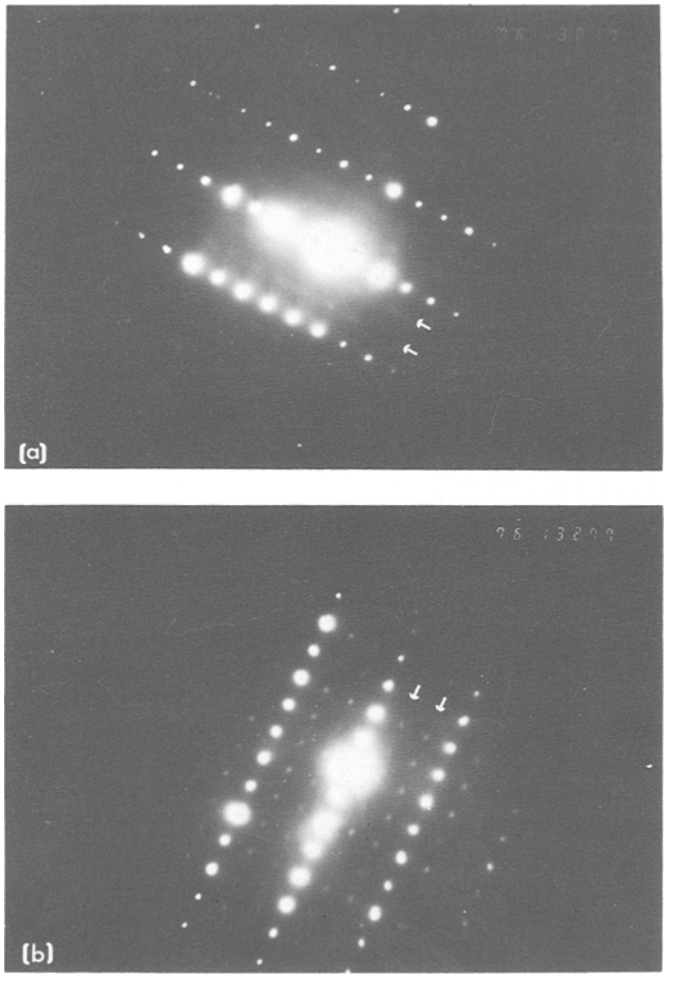

Figure 4 Electron diffraction photographs (1 1 0) of M6 β'' crystals (a) grown at 910° C and (b) grown at 980° C.

tations) in order to ascertain whether β'' (M6) is isostructural with willemite.

A criterion is needed to decide whether a crystal indexed on the large hexagonal cell really belongs to the hexagonal system or is actually rhombohedral. If the conditions for reflection are:

$$(-h + k + l) = 3n \qquad (3)$$

then the crystal is rhombohedral.

In willemite the zinc atoms are ordered on particular metal atom sites and the silicon atoms on others. Each column of metal atoms parallel with the screw triad axes is arranged [6] in the sequence Zn Zn Si Zn Zn Si, corresponding to the arrangement of beryllium and silicon in phenacite [5]. This arrangement means that the diffraction spots in layers hkl with $l = 3n$ are strong, while those in layers with $l \neq 3n$,

$\ldots h\,k\,1,\ h\,k\,2,\ h\,k\,4,\ h\,k\,5,\ h\,k\,7,\ h\,k\,8\ldots,$

have low intensities receiving structure factor contributions only as a result of differences in the scattering power between zinc and silicon, the oxygen atoms making no contribution to the structure factor for these particular reflections (i.e. those with l not a multiple of 3).

The additional weak reflections ($l \neq 3n$) in both β'' and willemite are referred to as "superlattice" reflections in this work although strictly speaking the term superlattice can only be applied where the disordered state also occurs.

3.3.2. Comparison of willemite and β'' (M6) electron diffraction patterns

The fundamental basal pattern (001) shows the characteristic regular hexagonal pattern of spots for both willemite (Fig. 5a) and β'' (Fig. 5b).

The β'' (1 2 0) electron diffraction pattern, obtained with the electron beam perpendicular to the hexagonal c-axis, is shown in (Fig. 5c). Starting

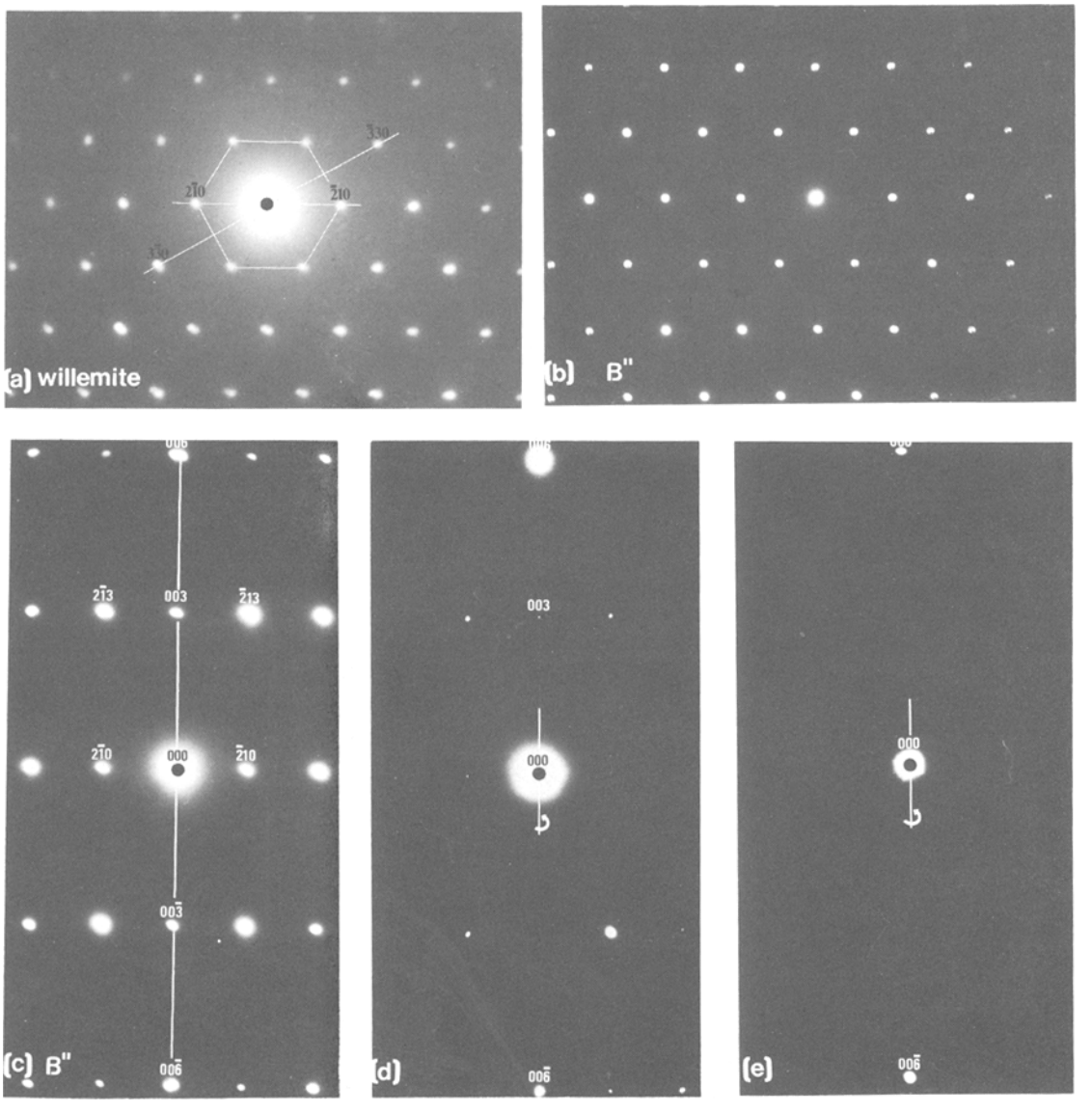

Figure 5 Willemite (a) and β'' (b) (001) electron diffraction photographs; (c) β'' (120) electron diffraction photograph, together with (d) and (e) progressive rotations from the (120) orientation of several degrees about the $00\bar{6}$–000–006 row.

from this (120) orientation, rotation of the β'' crystal a few degrees about its c-axis, which in effect involves rotating about the $00\bar{6}$–$00\bar{3}$–000–003–006 row of spots, results in the disappearance of all the spots not in this particular row. This is illustrated by progressive rotations of a few degrees in Figs. 5d and e.

However, as can be clearly seen in Fig. 5e, the 003 and $00\bar{3}$ diffraction spots also disappear out of this particular row, showing that the presence of these two reflections in the β'' (120) photograph is a result of multiple diffraction.

Starting from the (001) orientation, rotation about a suitable axis gives a systematic set of diffraction patterns, as a series of zones appear with their zone axes becoming parallel to the electron beam. There are two convenient axes (see Fig. 5a) to rotate about: (i) through the edges of the hexagon, e.g. about a row $2\bar{1}0$–000–$\bar{2}10$; and (ii) perpendicular to the faces of the hexagon, e.g. about a row $3\bar{3}0$–000–$\bar{3}30$. A representative selection of electron diffraction photographs obtained via these two systematic rotations are shown, respectively, in Figs. 6 and 7, where

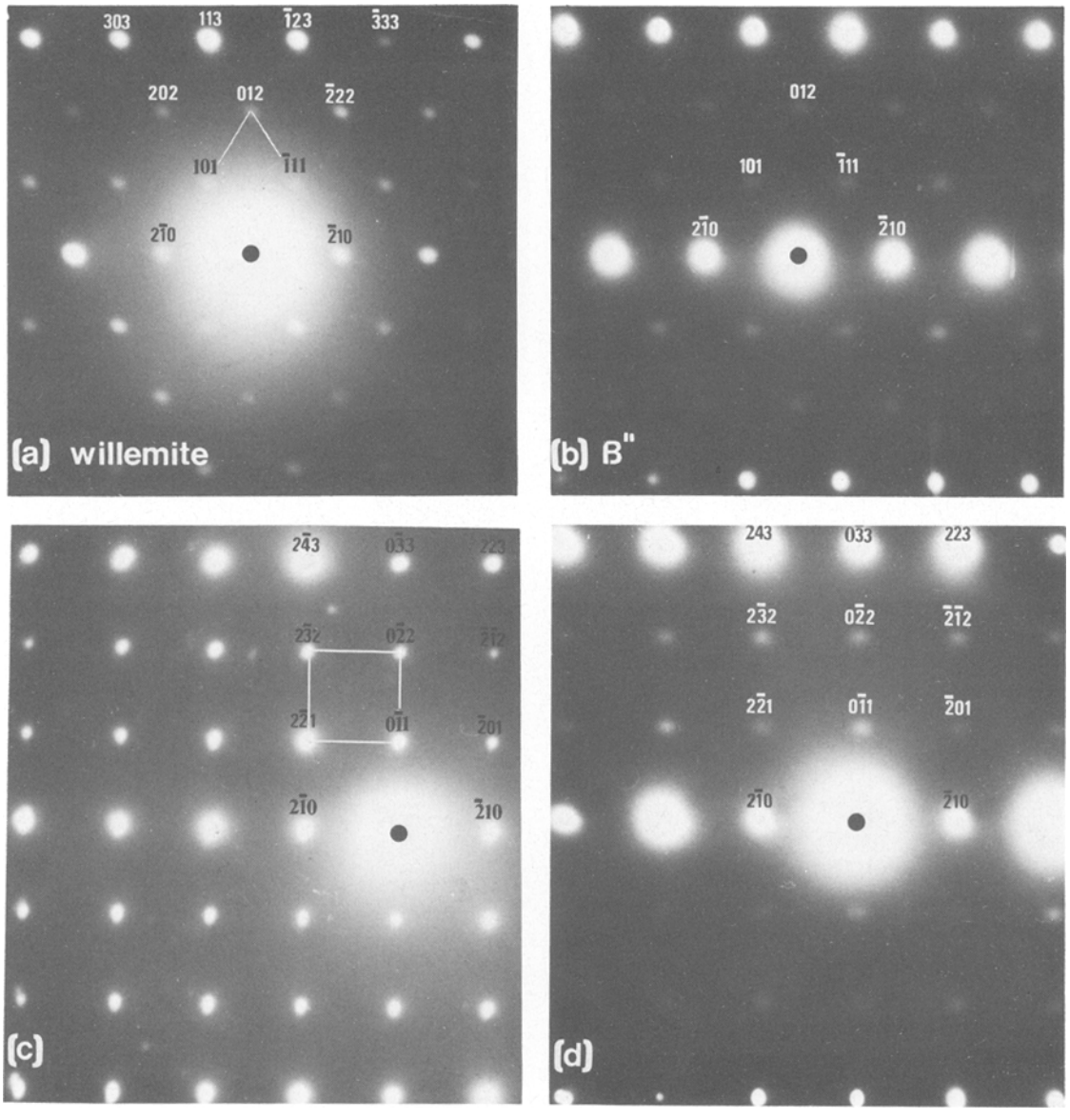

Figure 6 Electron diffraction photographs of willemite (left column) and β'' (right column): (a) and (b) orientation $(12\bar{1})$, (c) and (d) orientation $(12\bar{2})$, and (e) and (f) orientation (122).

willemite electron diffraction photographs (left column) are compared with the corresponding β''

3.3.2.1. $(12\bar{1})$ *diffraction patterns.* The willemite and β'' $(12\bar{1})$ diffraction patterns are identical in form, both with a 'v' pattern of "superlattice" spots (Figs. 6a and b). As might be expected the intensity of the β'' "superlattice" spots relative to the strong $l = 3n$ spots is markedly less than for the corresponding spots in willemite. That is, the difference between the (Mg + Al) and silicon scattering factors is less than the corresponding difference between the scattering factors of zinc and silicon.

3.3.2.2. (122) *diffraction patterns.* Both the willemite and β'' (122) patterns have the same almost square orthogonal array of "superlattice" spots (Figs. 6c and d).

3.3.2.3. $(12\bar{2})$ *diffraction patterns.* The willemite $(12\bar{2})$ pattern does not contain any "superlattice"

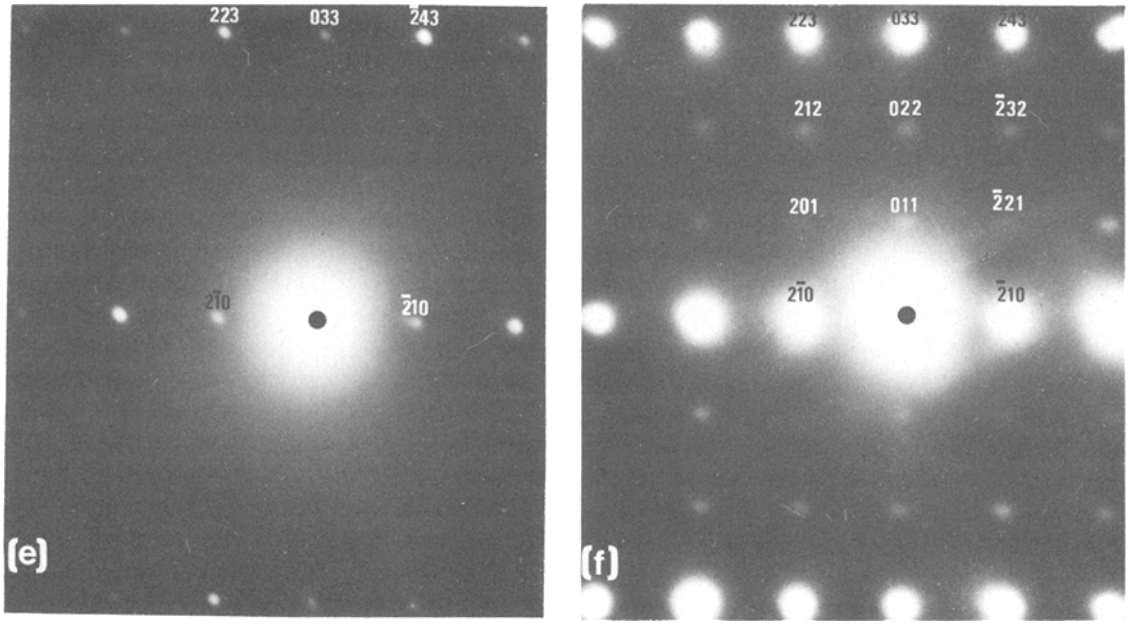

Figure 6 Continued.

spots (Fig. 6e) because the reciprocal lattice points with $l \neq 3n$ lying in this plane such as 212 and 011 have zero structure factor (i.e. their indices do not satisfy the rhombohedral criterion of $-h + k + l = 3n$).

However the corresponding β'' $(12\bar{2})$ pattern (Fig. 6f) does contain these "superlattice" spots not obeying the rhombohedral criterion giving an identical pattern of the β'' (122) orientation.

3.3.2.4. $(11\bar{1})$ *diffraction patterns.* The willemite $(11\bar{1})$ pattern contains diagonal rows of "superlattice" spots such as 101 and 202 (Fig. 7a).

The β'' $(11\bar{1})$ pattern (Fig. 7b) contains these same diagonal rows of superlattice spots obeying the rhombohedral criterion, but also contains other diagonal rows of superlattice spots such as $3\bar{1}2$ and $3\bar{2}1$ not obeying this criterion.

3.3.2.5. (*110*) *diffraction patterns.* The (110) reciprocal lattice plane involves a 90 degree rotation about the $3\bar{3}0$–000–$\bar{3}30$ axis of the basal plane. The willemite (110) pattern, shown schematically (Fig. 7c), contains diagonal rows of "superlattice" spots such as $\bar{1}11$ and $\bar{2}22$.

The β'' (110) pattern photograph (Fig. 7d) has an orthogonal array of "superlattice" spots. This array contains diagonal rows of spots obeying the rhombohedral criterion, and also diagonal rows of spots not obeying this criterion such as $2\bar{2}2$ and $1\bar{1}1$.

As can be clearly seen, in some orientations the patterns of "superlattice" spots in the willemite and β'' diffraction photographs are identical, e.g. (122) and $(12\bar{1})$. However, in the β'' (110) and $(11\bar{1})$ patterns there are some "superlattice" spots present that do not obey the rhombohedral criterion, and, in the (122) pattern none of the observed β'' "superlattice" spots obey the rhombohedral criterion.

4. Discussion

X-ray diffraction results gave no indication of any metal atom ordering, but this was not unexpected on the basis of the very small differences in X-ray scattering power between magnesium, aluminium, and silicon. By comparison the additional reflections due to the ordering of zinc and silicon are easily visible on X-ray diffraction photographs of Zn_2SiO_4.

Electron diffraction has proved sufficiently sensitive to detect weak "superlattice" reflections caused by metal atom ordering in the M6 β''. The annealing of the M6 glass at 910° C resulted in β'' crystals with only weak diffuse "superlattice" reflections indicative of partial ordering of the metal atoms. However on annealing at 980° C these reflections are discrete and reasonably sharp indi-

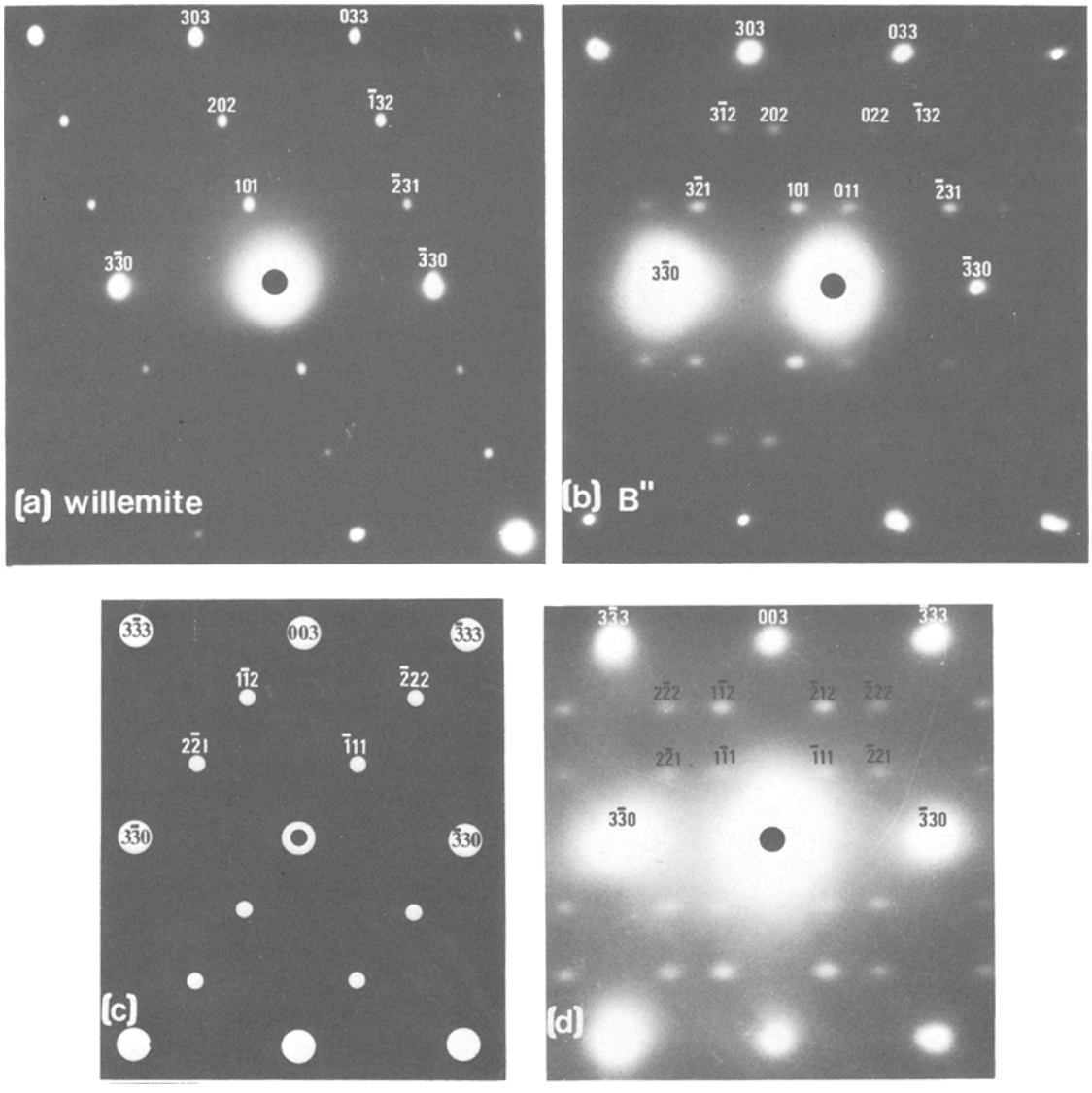

Figure 7 Electron diffraction photographs of willemite (left column) and β'' (right column): (a) and (b) orientation $(11\bar{1})$, (c) and (d) orientation (110). NB. Fig. 7 (c) is a schematic representation of the willemite (110) pattern.

cative of long range ordering. Now as the β'' crystallizes at a composition slightly different from but similar to the original quenched M6 glass, and the groupings of atoms in the glass (i.e. short range order) probably resemble the atomic structure of the metastable β'', the diffusion paths for the crystallization process are short. The change in the nature of the β'' "superlattice" spots clearly shown in Fig. 4 suggests that the diffusion paths for the glass → crystalline β'' transformation are shorter or approximately the same as the diffusion paths involved in the metal atom ordering process. Therefore with crystallization occurring at the lower temperature there is a tendency for the metal atoms to remain relatively disordered as they are in the glassy state, while, at the higher temperature the increased mobility of the atoms allows the metal atom ordering to take place as crystallization proceeds.

The ability of electron diffraction techniques to detect these very weak "superlattice" reflections in β''-magnesium sialon is due to:

(a) The significant difference in electron scattering factors between magnesium and silicon at angles where electron diffraction has an advantage over X-ray and neutron diffraction.

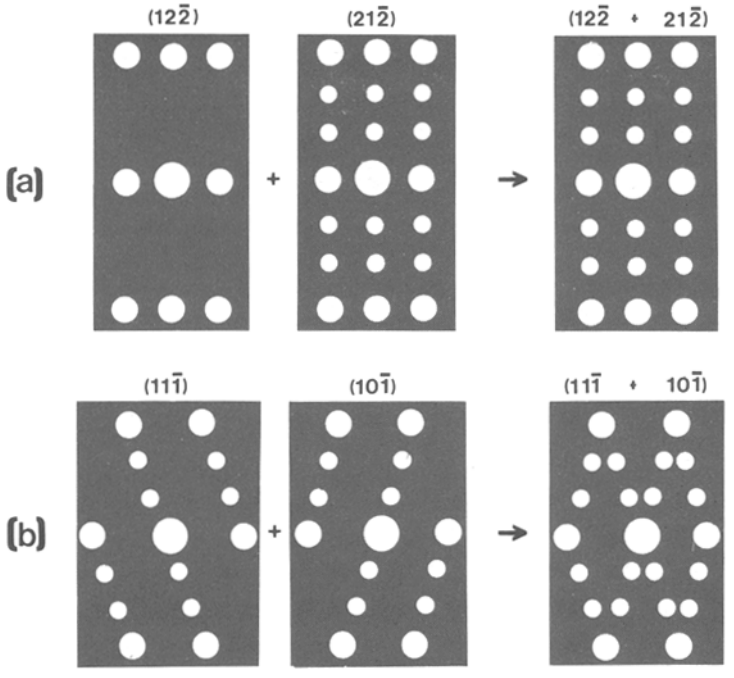

Figure 8 Schematic representations of the superimposition of the willemite electron diffraction patterns (a) (12$\bar{2}$) and (21$\bar{2}$), and (b) (11$\bar{1}$) and (10$\bar{1}$).

(b) Lack of background scatter in the electron diffraction photographs, which enables very weak reflections to show up against the surrounding clear film plate.

(c) Multiple diffraction, which in general enhances weak reflections relative to the strong reflections.

The increased % ionic nature of the bonding in the high magnesium content M6 β'' magnesium sialon compared with β' sialons may also contribute to the advantages that electron diffraction has over X-ray diffraction in detecting the metal atom ordering. The higher the degree of ionicity in the β'' bonding. the less sensitive X-ray diffraction techniques will be in detecting β'' metal atom ordering because Mg^{2+}, Al^{3+} and Si^{4+} ions are isoelectronic and X-rays are scattered only by the extra-nuclear electrons, whereas electrons are scattered by the nucleus as well as the extra-nuclear electrons.

A number of significant conclusions may be drawn from a comparison of the willemite and M6 β'' electron diffraction data.

(i) The patterns of β'' and willemite are of similar dimensions confirming the close similarity in cell dimensions for the two structures.

(ii) Reflections ($h\ k\ l$) for $l \neq 3n$ are weak compared with those for $l = 3n$. In willemite this effect results from the ordering of zinc and silicon atoms along the c-axis in the sequence . . . Zn Zn Si Zn Zn Si . . . . Exactly the same phenomenon is observed for the M6 β'' which confirms a similar form of arrangement of atoms along the c-axis, i.e. (Mg, Al) (Mg, Al) Si (Mg, Al) (Mg, Al) Si . . . , and which result in a tripling of the c-dimension of the hexagonal cell. Also, as one might expect, the relative intensities of the $l \neq 3n$ to the $l = 3n$ reflections are weaker in β'' than in willemite because of the smaller differnece in scattering power between the metal atoms present.

(iii) Although there is a remarkable similarity in the form of diffraction patterns obtained from the two materials there are also rather subtle differences. The rhombohedral symmetry of willemite means that when indexing using the larger hexagonal cell only reflections for which $-h + k + l = 3n$ are allowed. However, "superlattice" reflections violating this condition are present in β''. The 003 and 00$\bar{3}$ reflections are allowed according to the rhombohedral criterion but their appearance in the β'' (120) pattern has been shown to be caused by multiple diffraction. As the 003 reflection is not observed in X-ray diffraction photographs of willemite and phenacite it may be that the β'' 003 and 00$\bar{3}$ reflections are too weak to be observed even in electron diffraction.

The possible occurrence of oxygen : nitrogen ordering in the M6 β'' would not be expected to produce reflections strong enough to be visible as the difference in scattering factors for electrons

between oxygen and nitrogen is so small (the O/N ratio in β'' is approximately 7/1).

A possible explanation for the differences between the willemite and β'' electron diffraction photographs is that the M6 β'' has in fact the true willemite structure, but ordered microdomains involving twinning are resulting in reflections not satisfying the rhombohedral condition appearing in the electron diffraction photographs.

For example, if two ordered microdomains, each with the willemite structure, exist adjacent to each other and are related by a 60 degree rotation about the hexagonal c-axis, then the observed electron diffraction photograph taken from this volume of crystal would consist of two superimposed patterns, one from each twinned microdomain. The effect this would have on the observed electron diffraction patterns is illustrated in the following two examples of the superimposition of pairs of electron diffraction patterns related to each other by a sixty degree rotation about the willemite reciprocal lattice c^*.

The superimposition of the willemite $(1\,2\,\bar{2})$ and $(2\,1\,\bar{2})$ electron diffraction patterns is schematically illustrated in Fig. 8a. Such a superimposition results in the orthogonal "superlattice" spots of pattern $(2\,1\,\bar{2})$ appearing on the $(1\,2\,\bar{2})$ pattern which does not have any such "superlattice" spots. Compare $(1\,2\,\bar{2} + 2\,1\,\bar{2})$ with the β'' pattern of Fig. 6d.

The superimposition of the willemite $(1\,1\,\bar{1})$ and $(1\,0\,\bar{1})$ electron diffraction patterns is shown Fig. 8b. Such a superimposition results in the diagonal rows of "superlattice" spots of pattern $(1\,0\,\bar{1})$ appearing as extra spots on the $(1\,1\,\bar{1})$ pattern. Compare $(1\,1\,\bar{1} + 1\,0\,\bar{1})$ with the β'' pattern of Fig. 7b.

Both these examples show how such twinning could cause the appearance of diffraction spots apparently not obeying the rhombohedral criterion in the β'' electron diffraction photographs $(1\,2\,\bar{2})$ and $(1\,1\,\bar{1})$ and likewise in $(1\,1\,0)$.

Although the existence of microdomain twinning is hypothetical at this stage, the driving force for the formation of such twins could be a reduction in overall lattice strain energy by the reversal of shear distortion across adjacent microtwins, analogous to that found in vanadium carbide [13]. The large level of magnesium substitution in this metastable M6 β'' does introduce considerable strain into the crystal lattice, as shown by its rapid transformation into a stable phase assemblage (mainly forsterite) at temperatures over 1120° C [11].

5. Conclusion

The electron diffraction studies of this work have confirmed the existence of metal atom ordering in a high magnesium content β''-magnesium sialong as suggested first by Wild *et al.* [10]. This involves the ordering of magnesium and aluminium with respect to silicon in a similar way to phenacite-type ordering in willemite.

Whether the structure of the M6 β'' is identical to that of willemite and the unaccounted for extra spots are a result of "ordered microdomains" is as yet unproven and more work is required to resolve this. Such "microdomain twinning" would normally be visible (imaged) in dark field if the "superlattice" reflections were of sufficiently large intensity and the domain size was easily resolvable. However there is no doubt that the β'' and willemite structures aere very nearly identical.

References

1. D. HARDIE and K. H. JACK, *Nature* **180** (1957) 332.
2. S. WILD, P. GRIEVSON and K. H. JACK, *Spec. Ceram.* **5** (1972) 385.
3. K. H. JACK, *J. Mater. Sci.* **11** (1976) 1135.
4. R. J. LUMBY, B. NORTH and A. J. TAYLOR, *Spec. Ceram.* **6** (1975) 283.
5. W. L. BRAGG and W. H. ZACHARIASEN, *Z. Krist.* **72** (1930) 518.
6. C. HANG, A. SIMONOV and N. V. BELOV, *Sov. Phys. Crystallogr.* **153** (1970) 387.
7. L. GILLOT, N. COWLAN and G. E. BACON, *J. Mater. Sci.* **16** (1981) 2263.
8. J. A. GARD, "Weak reflections in electron-diffraction patterns", Proceedings of the 2nd European Congress on Electron Microscopy, Delft, Vol. 1, August 1960, p. 203.
9. M. S. Y. BHATTY, J. A. GARD and F. P. GLASSER, *Mineral. Mag.* **37** (1967) 267.
10. S. WILD, G. LENG-WARD and M. H. LEWIS, *J. Mater. Sci.* **16** (1981) 1815.
11. G. LENG-WARD, PhD thesis, Polytechnic of Wales, (1983).
12. "International Tables for X-ray Crystallography", Vol. 1 (Kynoch Press, Birmingham, 1969) p. 18.
13. M. H. LEWIS, *Phil. Mag.* **31** (1975) 173.

Received 8 August
and accepted 18 August 1983